Available online at www.sciencedirect.com
ScienceDirect
Trans. Nonferrous Met. Soc. China 26(2016) 272−281
Transactions of Nonferrous Metals Society of China
www.tnmsc.cn

Microthermokinetic study of xanthate adsorption on impurity-doped galena

Li-hong LAN[1], Jian-hua CHEN[2], Yu-qiong LI[2], Ping LAN[1], Zhuo YANG[1], Guang-yong AI[1]

1. Guangxi Colleges and Universities Key Laboratory of Chemical and Biological Transformation Process Technology, School of Chemistry and Chemical Engineering, Guangxi University for Nationalities, Nanning 530006, China;
2. School of Resources and Metallurgy, Guangxi University, Nanning 530004, China

Received 6 January 2015; accepted 15 July 2015

Abstract: Six kinds of galena with different impurities were synthesized and the effects of impurities on the floatability of galena were investigated. The thermodynamic and kinetic parameters on the galena surface were measured using microcalorimetry, and the adsorption configuration and energy of butyl xanthate on the surfaces of galena with different impurities were simulated by density functional theory. Flotation experiments showed that Ag and Bi significantly promoted the recovery of galena, while Zn, Sb, Mn, and Cu reduced the recovery of the flotation. Microthermokinetic results indicated that the absolute value of xanthate adsorption heat was directly proportional to the flotation recovery of galena. Adsorption heat and reaction rate coefficients of xanthate on galena containing Ag or Bi were larger than those on pure galena, but smaller on galena containing Cu or Sb. Additionally, the relationship between the heat of unsaturated adsorption of xanthate and the adsorption energy of impurity atom on galena surface was investigated.

Key words: galena; impurity effect; floatation; xanthate; adsorption; microcalorimetry; density functional theory

1 Introduction

The flotation results in practice show that the flotation behavior of sulfide minerals is related to their sources. Natural sulfide minerals generally contain impurities in lattices, and the type and contents of impurities, mainly controlled by surrounding of the crystallization of mineral, are varied in different origins. For example, natural galena may contain Ag, Cu, Zn, Fe, Sb, Bi, Mn, In and other impurities [1]. Natural sphalerite often contains Fe, Cd, Ge, Ga, In, Hg, Mn and other impurities [2]. Natural pyrite contains Co, Ni, As, Cu, Au, Zn, Bi, Hg, Bi and other impurities [3−5]. The presence of impurities in lattices changes the physical and chemical properties of sulfide minerals, thus influencing their floatability. It has been found that Ag, Bi and Cu impurities improve the floatability of galena, while Zn, Mn and Sb impurities reduce its floatability [1].

The influences of lattice impurities on the crystal structures and properties of pyrite [6,7] and sphalerite [8,9] were discussed by density functional theory (DFT). CHEN et al [10] synthesized impurity-doped ZnS and investigated the influence of Fe, Mn, Cu and Cd impurities on the flotation behaviors of sphalerite. For galena, CHEN et al [11] explored the effect of impurities on the electronic structures and semiconductor properties, and LAAJALEHTO et al [12] investigated the influence of antimony impurity on the flotation behavior. However, the microthermokinetics of impurity-bearing galena flotation has not been reported.

Microcalorimetry technique can accurately detect the Nava level, thermal power, and 10^{-7} J magnitude of the energy. The temperature-controlled precision can reach 10^{-4}−10^{-5} °C. The thermodynamics and kinetics information of flotation regent adsorption on the mineral surface can be accurately gathered using this method. In the earlier years, MELLGREN [13] measured the heat of adsorption of ethyl xanthate on the untreated galena. In addition, the kinetics and thermochemistry of the xanthate adsorption reaction on pyrite and marcasite were examined by HAUNG and MILLER [14]. The heats of adsorption of 2-mercaptobenzoxazole (MBO) on

Foundation item: Projects (51464006, 51164001) supported by the National Natural Science Foundation of China; Project (GJR201147-12) supported by Guangxi Higher Education Institutes Talent Highland Innovation Team Scheme, China; Project (2012MDZD038) supported by the Key Scientific Research Project of Guangxi University for Nationalities, China
Corresponding author: Jian-hua CHEN; Tel: +86-771-3232200; E-mail: jhchen1971@sina.com
DOI: 10.1016/S1003-6326(16)64115-8

chalcocite, 2-mercaptobenzothiazole (MBT) on galena and 2-aminothiophenol (ATP) on sphalerite have been measured [15]. Meanwhile, MAIER et al [15] also measured the heats of adsorption of xanthate on the surface of galena, sphalerite and chalcocite. Recently, we have investigated the heat of adsorption and kinetics parameters in the process in which dithiophosphate and diethyldithiocarbamate were absorbed on the surface of galena and pyrite surfaces [16]. However, thermodynamics behaviors of the adsorption of reagent molecules on sulfide minerals bearing impurities have not been reported.

Synthetic Fe-doped sphalerites are usually used to investigate the effect of iron content on flotation behavior of sphalerite [10,17,18]. The influences of Ag, Bi, Sb and Zn impurities on the electrochemical adsorption of butyl xanthate on a galena surface were also investigated [19]. In this work, six kinds of galenas with different impurities were synthesized via chemical precipitation and the effects of impurities on the floatability of galena were studied. The thermodynamic and kinetic parameters of *n*-butyl xanthate (BX) adsorbed on galena containing different impurities were measured by using microcalorimetry technique. In addition, the computational simulation was used to obtain the adsorption structure of xanthate on the impurity-doped galena surface.

2 Experimental

2.1 Chemicals and characteristics of minerals

The chemical reagents, including lead acetate trihydrate ($Pb(CH_3COO)_2·3H_2O$), sodium sulfide nonahydrate ($Na_2S·9H_2O$), silver nitrate ($AgNO_3$), zinc chloride ($ZnCl_2$), copper sulfate ($CuSO_4·5H_2O$), antimony trichloride ($SbCl_3$), bismuth nitrate pentahydrate ($BiCl_3·5H_2O$), and manganese(II) chloride tetrahydrate were purchased from Sinopharm Chemical Reagent Company (Shanghai, China). The chemicals were analytical grade. Single crystal galena sample was obtained from Fankou Mine, Guangdong Province, China. Multi-element analysis indicated that the galena sample was of high purity with only traces of Sb and Co compounds, which was confirmed by the results of X-ray diffraction (XRD) examination. Sodium butyl xanthate (BX) was synthesized through reacting butyl alcohol with sodium hydroxide and carbon disulfide.

2.2 Synthesis of impurity-doped galena

Pure galena was synthesized using sodium sulfide as sulfur source and lead acetate as lead source. The theoretical molar ratio of these two compounds in the complete reaction conditions is 1:1. To completely precipitate Pb^{2+}, slight excess of sodium sulfide is needed. The synthesis process is as follows: Firstly, 74.8 g of $Pb(CH_3COO)_2·3H_2O$ was dissolved in proper amount water in a 5000 mL beaker to obtain solution A. Secondly, 52.8 g of $Na_2S·9H_2O$ was dissolved in proper amount of water to obtain solution B. Finally, solution B was added to solution A with stirring to give a black galena. The impure galena was prepared by the reaction of sodium sulfide with lead acetate and metal X salts (acting as impurities, where X refers to Ag, Cu, Zn, Bi, Sb, and Mn). Lead acetate trihydrate and metal X salts were dissolved in deionized water, followed by the addition of sodium sulfide solution. The resultant mixture was stirred for 12 h and then filtered, and the black solid was washed with a lot of water. Finally, the solid product was dried in oven at 90 °C for 48 h. The content of impurities was determined by chemical analysis [20]. The doped samples showed that the mass fractions of Ag, Zn, Cu, Sb, Bi and Mn impurities were 4.98%, 4.97%, 4.98%, 5.01%, 5.02% and 4.99%, respectively, which are within the scope of limited content. The qualified samples were ground to 75−150 μm and used for flotation examinations. The samples for XRD characterization and microcalorimetry examination were ground to be smaller than 45 μm.

2.3 Determination of specific surface area

Surface areas of the minerals were determined with 5-point BET (Brunauer–Emmett–Teller) method using JW−004 type BET nitrogen adsorption specific surface area apparatus (JWGB Sci. & Tech. Company, Beijing, China). Before measurement, 2 g sample of each mineral was dried for 24 h under the vacuum and helium was used for the determination of the dead-volume and nitrogen as the adsorbent gas.

2.4 Flotation test

An XFGC−80 model aeration hanging cell flotation machine (Changchun Prospecting Machinery Manufacturer, China) was used in the flotation tests. The effective capacity of the flotation cell was 40 mL. The prepared mineral samples (2.2 g) were immersed in a weak acid solution with pH of 5−6 to remove the oxidized layer from the surface. Then, the ultrasonic cleaning was conducted for 10 min. After removing the supernatant, the samples were washed thoroughly with distilled water, and transferred into the flotation cell. In the flotation, butyl xanthate was used as collector, and methyl-iso-butyl-carbinol (MIBC) was used as frother. After conditioning with butyl xanthate (1 mmol/L) for 5 min, 0.02 mL MIBC was added and conditioned for another 5 min. An impeller speed of 2502 r/min was maintained throughout the flotation test. The froth product and tailing samples were collected, dried and weighed.

2.5 Microcalorimetric measurement

The microcalorimetric measurements were accomplished with a RD496−III type microcalorimeter (Mianyang Zhongwu Thermal Analysis Instrument, China), which is displayed in Fig. 1(a). Sample cell and stainless steel sleeve are displayed in Fig. 1(b). The detailed description about the structure and technical parameters of this calorimeter has been reported in Ref. [21]. The temperature was kept constant at 25 °C during examinations. Heat of the adsorption reaction was measured in an isothermal reactor. Firstly, 1.0 g of mineral sample (<45 μm) was immersed in a weak acid solution with pH of 5−6 to remove the oxide layer from the surface. Then, the ultrasonic cleaning was conducted for 10 min. After removing the supernatant from the container, the samples were washed thoroughly with distilled water several times to pH 7, and then transferred into a 50 mL Erlenmeyer flask. Distilled water was added to the Erlenmeyer flask to produce a 20 mL mine pulp sample solution. The concentration of xanthate solution was 0.2 mmol/L. Next, 1 mL xanthate solution and 1 mL mineral samples were injected respectively into a 3 mL small sample cell and a 6 mL large sample cell using a microinjector. The small cell was inserted into the large cell, and then put into a 15 mL stainless steel sleeve. The sealed stainless steel sleeve was placed in the microcalorimeter container. The reaction parameters were set. When baseline was stable, the small cell was pierced and xanthate solution flowed into the large cell. The XB was mixed with mineral samples in the large cell. The thermal effect was then automatically recorded.

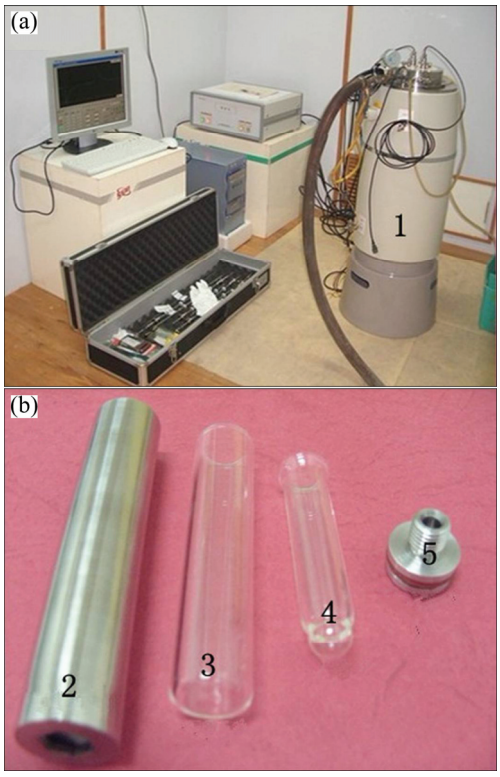

Fig. 1 RD496−III type microcalorimeter (a) and sample cell and stainless steel sleeve (b): 1—Microcalorimeter; 2—Stainless steel sleeve; 3—Large sample cell; 4—Small sample cell; 5—Cap of stainless steel sleeve

2.6 Computational method

The simulations of collector adsorption have been done using Cambridge Serial Total Energy Package (CASTEP) developed by PAYNE et al [22], which was a first-principle pseudopotential method based on DFT. In DFT calculations, plane wave (PW) basis sets and ultrasoft pseudopotentials were used. The exchange correlation functional used was GGA-PW91 [23,24]. The interactions between valence electrons and ionic core were represented by ultrasoft pseudopotentials. Valence electron configurations considered in this study included: Pb $5d^{10}6s^26p^2$, S $3s^23p^4$, C $2s^2\ 2p^2$, O $2s^22p^4$, H $1s^1$, Ag $4d^{10}4s^1$, Bi $4f^{14}5d^{10}6s^26p^3$, Sb $4d^{10}5s^25p^3$, Cu $3d^{10}4s^1$, Zn $3d^{10}4s^2$ and Mn $3d^54s^2$ states. The PW cutoff energy of 280 eV was used for galena calculations. The Brillouin zone was sampled with Monkhorst and Pack special k points of a 1×2×1 grid for PbS surface calculations [25], which showed that the cutoff energy and the k points meshes were sufficient for the system. For self-consistent electronic minimization, the Pulay density mixing technique was used with the convergence tolerance of 2.0×10^{-6} eV/atom. The energy tolerance, the force tolerance, and the displacement tolerance were 2.0×10^{-5} eV/atom, 0.08 eV/Å and 0.002 Å, respectively. The optimization of xanthate was calculated in a 15 Å × 15 Å × 15 Å cubic cell and the optimization was performed at the gamma point in the Brillouin zone.

The slab thickness of galena surface and vacuum thickness were tested in our previous work [26,27]. Thus, we constructed a (4×2) PbS (100) surface with eight atomic layers and vacuum thickness of 15 Å. The three outermost atomic layers of the substrate on the PbS surface were allowed to relax while the five bottom-most atomic layers of the substrate were fixed to the bulk coordinates in the adsorption calculations. Side view and top view of (4×2×1) galena (100) surface are shown in Fig. 2. Substitution position of impurity atom and side length of galena surface are shown in Fig. 2(b). Various impurity defect surface models are formed when lead atom is replaced by different impurity atoms.

The adsorption energy of xanthate on galena surface was calculated using Eq. (1):

$$\Delta E_{ads} = E_{X/slab} - E_X - E_{slab} \quad (1)$$

where ΔE_{ads} is the adsorption energy, E_X is the energy of the xanthate, E_{slab} is the energy of the perfect PbS or

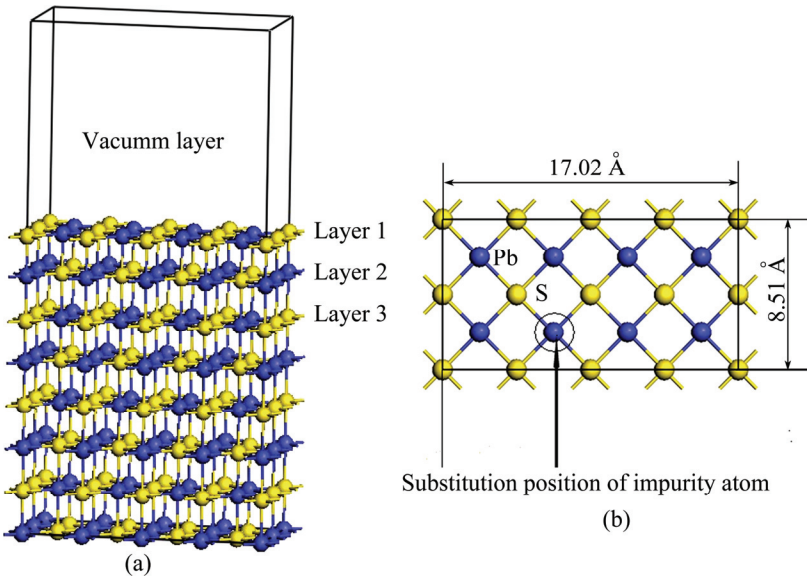

Fig. 2 Slab model of (4×2×1) galena (100) surface with 15 atomic layers and vacuum thickness of 15 Å: (a) Side view; (b) Top view

impurity-doped PbS, and $E_{X/slab}$ is the energy of the xanthate adsorbed on mineral surface. The more negative value of ΔE_{ads} indicates the stronger adsorption of xanthate.

3 Results and discussion

3.1 X-ray diffraction characterization of impurity-doped galena

The XRD patterns of natural and synthetic impurity-doped galena are displayed in Fig. 3. It is shown that in 2θ range of 10°−70° there are seven obvious characteristic peaks: 26.04°, 30.16°, 43.16°, 51.04°, 53.52°, 62.58° and 69.06°. These peaks can be attributed to the galena-type face-centered cubic structure of PbS. This is consistent with the standard XRD data (PDF card No. 65−9496). No impurity peaks were detected, indicating that no separate impurity phase formed.

Figure 3 also shows that there exist two peaks in 2θ of range 20°−25° with Sb-, Bi- and Ag-doped galena. These peaks can be attributed to $Pb(SO)_4$. In addition, different impurity-doped galenas have many different ratios of signal to noise and different peak ratios compared with natural galena, which indicate that there are some isolated inclusion phases containing the "dopant" species on the synthesized sample surface. This is likely to be a source of the specific element in reality during processing. There are many examples of very minor phases oxidizing, dissolving and re-adsorbing on the host mineral surface at surface concentrations much higher than those present in bulk. Cu from sulfide inclusions in pyrite is a classic example. So, the existence of additional phases is as a positive and closer to a real situation.

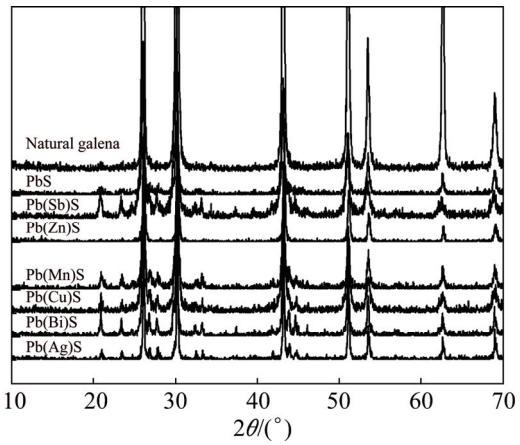

Fig. 3 XRD patterns of natural and synthetic impurity-doped galena

Lattice constant of impurity-doped galena can be obtained using MDI Jade 5.0 program. The measured and calculated lattice constants of impurity-doped galena shown in Table 1 indicate that the lattice constant of synthetic PbS is 0.5926 nm, which is very close to 0.5928 nm of the natural galena and the literature value of 0.5924 nm [28]. Moreover, the lattice constant of galena decreases due to the presence of Ag, Cu, Zn and Mn impurities, whereas it increases in the presence of Bi and Sb impurities. These results are consistent with the calculated values using DFT method. These observations indicate that the crystal model and calculation parameters used in this study are reliable.

3.2 Effects of impurities on galena flotation

3.2.1 Flotation behaviors of synthetic and natural galena

There are great differences between the flotation of synthetic and natural galena. The recovery of natural

Table 1 Lattice constants of PbS with impurity

Mineral	Lattice constant/nm		
	Measured	Calculated	Ref. [28]
Natural galena	0.5928		0.5924
PbS	0.5926	0.6018	
Pb(Ag)S	0.5923	0.6008	
Pb(Zn)S	0.5918	0.5958	
Pb(Cu)S	0.5920	0.5858	
Pb(Sb)S	0.5931	0.6130	
Pb(Bi)S	0.5929	0.6250	
Pb(Mn)S	0.5923	0.5760	

galena is generally larger than 90%, while that of synthetic galena flotation is approximately 35% under the same flotation conditions. According to the previous XRD results, the poor flotation was not due to the phase and crystal structure of synthetic galena, but due to the chemical precipitation method for synthetic galena. Therefore, there are large differences between natural and synthetic galena for the surface properties and adsorption capacity.

The first difference between synthetic and natural galena was their specific surface areas. The test results showed that the specific surface areas of the synthetic and natural galena were 9.35 and 0.38 m^2/g (for the samples finer than 45 μm), respectively. The specific surface area of synthetic galena was about 25 times larger than that of the natural galena, which led to more reagents needed in the flotation of synthetic galena. This was the same as the reported result that the flotation of synthetic magnetite was poorer compared with that of the natural magnetite [29]. In addition, the consumption of collector used for the flotation of synthetic magnetite was 5 times larger than that of natural magnetite due to the larger specific surface area of synthetic magnetite.

There was also difference between the surface adsorption activity of the synthetic and natural galena. Microcalorimetric test results showed that the adsorption heat of natural galena was 2.976 J/m^2, while that of the synthetic galena was only −0.28 J/m^2. It was suggested that when xanthate was used as the collector, the adsorption activity of natural galena was 10 times greater than that of synthetic galena. Our observations indicated that in order to get a better flotation, a larger collector concentration is required to float the synthetic galena.

3.2.2 Effects of impurities on flotation recovery of synthetic galena

The effects of xanthate on the flotation recovery of synthetic galena containing impurities are shown in Fig. 4. The floatability of galena was different due to different types of impurities and decreased in the following order: Ag>Bi>pure galena>Mn>Cu>Sb>Zn.

The results indicated that Ag and Bi elements could improve the flotation of galena, while Zn, Sb, Mn and Cu impurities inhibited the flotation of galena.

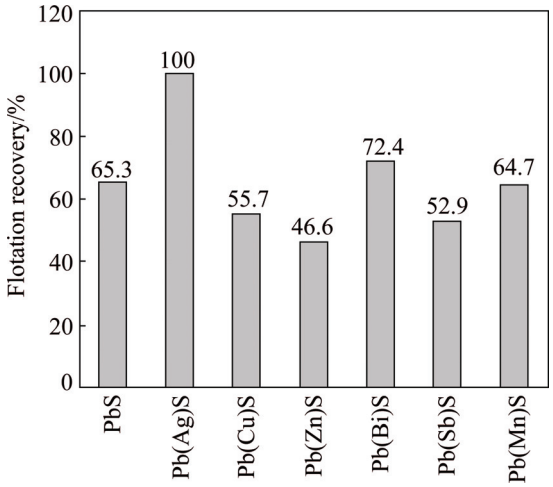

Fig. 4 Effects of impurities on flotation recovery of synthetic galena at butyl xanthate concentration of 1 mmol/L

3.3 Adsorption of xanthate on perfect galena surface

The adsorption configurations of CH_3OCS_2 and $C_4H_9OCS_2$ on the perfect galena (100) surface were simulated and optimized using the first-principle method based on DFT (Fig. 5). The numbers in Fig. 5 are Pb—S bond lengths. It can be seen that the two sulfur atoms of xanthate molecules were bonded to the two Pb atoms of the galena surface. The bond length between a single bond S and Pb (S1—Pb1) was shorter than that between the double bond S and Pb (S2—Pb2), suggesting that the S1—Pb bond was stronger than the S2—Pb2 bond. The adsorption energies of butyl and methyl xanthates on the galena surface were −67.02 and −71.33 kJ/mol, respectively, and the adsorption configurations were very similar with nearly equal corresponding S—Pb bond lengths. Therefore, the methyl xanthate was selected to simulate the adsorption of xanthate molecules on the surface of galena.

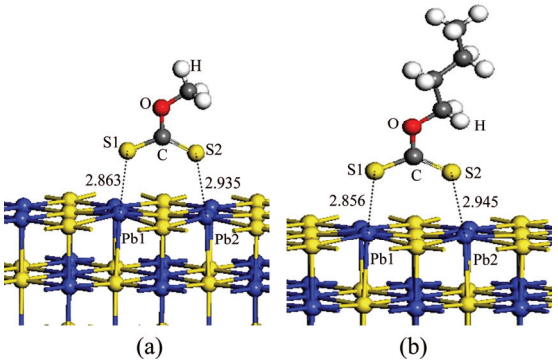

Fig. 5 Configurations of CH_3OCS_2 (a) and $C_4H_9OCS_2$ (b) adsorptions on galena (100) surface (unit: Å)

Figure 6 shows the equilibrium heat of adsorption of xanthate (ΔH) on synthetic pure galena surface at various xanthate concentrations (c_{BX}). It was suggested that the heat of adsorption increased steadily with the increase of the xanthate concentration. According to Fig. 6, it could be known that the adsorption of xanthate on the synthetic galena surface did not reach saturation under lower xanthate concentration (0.1 mmol/L). Therefore, the adsorption density of xanthate on the galena surface could be estimated by comparing the measured heat of adsorption with calculated adsorption energy.

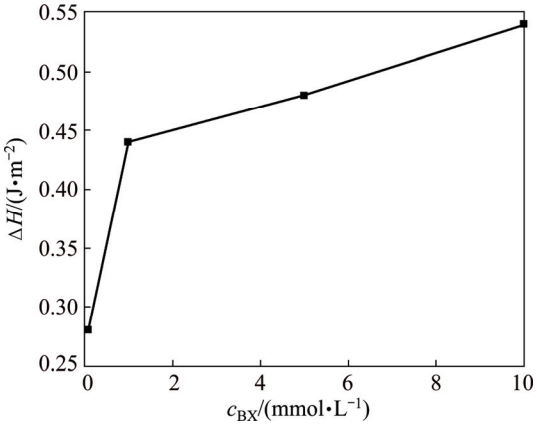

Fig. 6 Heat of adsorption of BX on synthetic galena as function of XB concentration

The 4×2×1 galena surface model gave a surface area of 1.448×10^{-18} m^2, which provided four adsorption sites for xanthate molecule. Based on this surface area, there would be 2.8×10^{18} adsorption sites for xanthate molecule per square meter of galena surface. The calculation gave a BX adsorption energy of −67.02 kJ/mol on the galena surface, equivalent to −0.31 J/m^2 for a xanthate molecule adsorption energy on galena surface. Compared with the measured heat of adsorption of −0.28 J/m^2 (ignoring the entropy change), the adsorption layer of xanthate on the galena surface could be estimated to be approximately 0.9 monolayer.

3.4 Adsorption of xanthate on impurity-bearing galena surface

The adsorption configurations of xanthate on the impurity-bearing galena surface are shown in Fig. 7. The numbers in the figure are Pb—S bond lengths. It is demonstrated that the single bond S was bonded to the impurity atom, and the double bond S was bonded to the Pb atom on the galena surface. The calculated adsorption energy (ΔE_{ads}) and the solubility product of metal ethyl xanthate (pK_{sp})[30] are shown in Table 2. Zn and Cu impurities had little effect on the adsorption energy; whilst Ag, Mn, Sb and Bi impurities could reduce the adsorption energy. The most significant reduction was observed in Bi impurity. These results indicated that

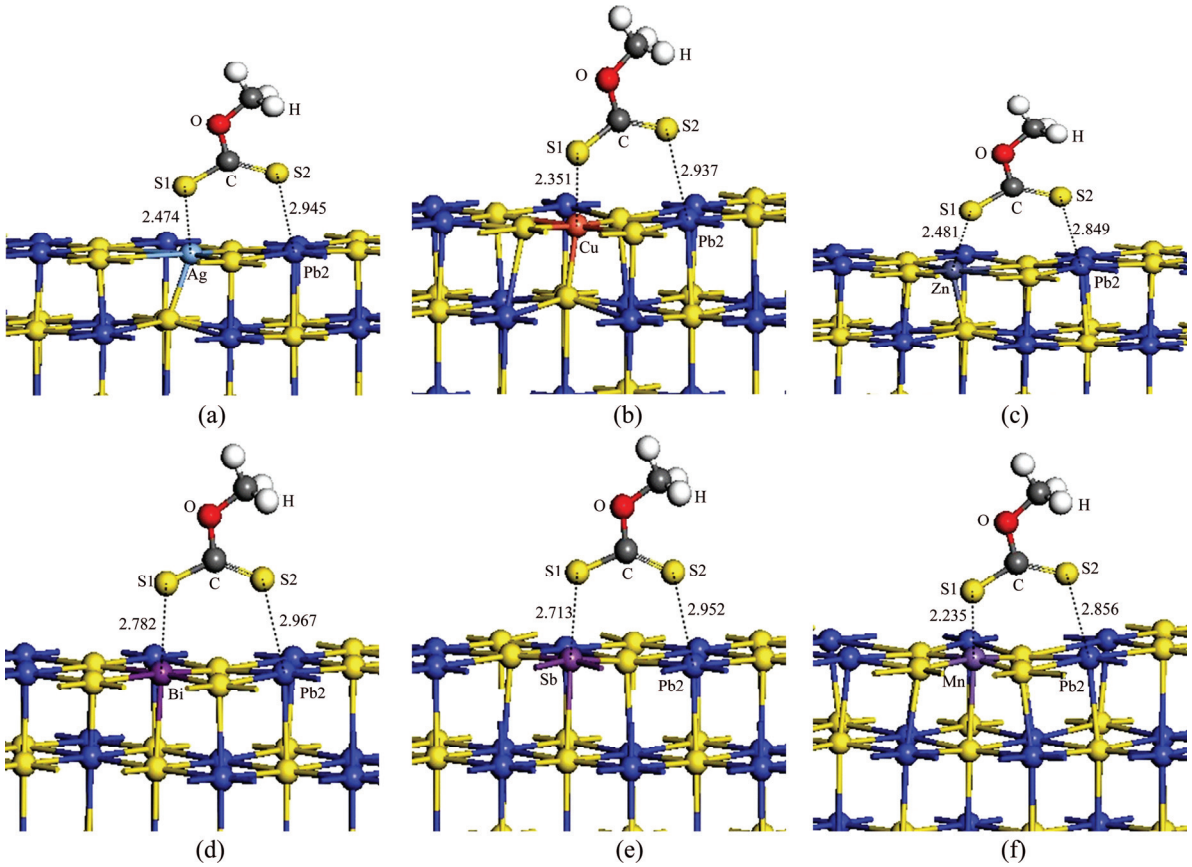

Fig. 7 Adsorption configurations of xanthate on Ag- (a), Cu- (b), Zn- (c), Bi- (d), Sb- (e) and Mn-bearing (f) galena surfaces (unit: Å)

Table 2 Simulated adsorption energies of xanthate on impurity-bearing galena surface and pK_{sp} of metal ethyl xanthate

Mineral	Adsorption energy, ΔE_{ads}/(kJ·mol^{-1})	Ethyl xanthate metal salt	pK_{sp}
PbS	−71.33	$C_2H_5OCS_2Pb$	16.77
Pb(Ag)S	−92.17	$C_2H_5OCS_2Ag$	18.1
Pb(Bi)S	−212.01	$C_2H_5OCS_2Bi$	~30.9
Pb(Cu)S	−74.90	$C_2H_5OCS_2Cu$	19.28
Pb(Mn)S	−198.89	$C_2H_5OCS_2Mn$	−
Pb(Sb)S	−199.27	$C_2H_5OCS_2Sb$	~24
Pb(Zn)S	−73.07	$C_2H_5OCS_2Zn$	8.31

smaller adsorption energy corresponded to larger pK_{sp} and smaller solubility of metal salts. For instance, Bi provided the smallest adsorption energy and the largest pK_{sp} values. The pK_{sp} value of zinc xanthate was minimal, so it was easily dissolved, which suggested that zinc impurity was not conducive to flotation for galena.

3.5 Microheat of adsorption of xanthate on impurity-doped galena surface

Figure 8 shows the microcalorimetric curves of BX adsorption on galena containing various impurities. Curves related to galena containing Ag, Bi, Mn, Cu, Zn and Sb impurities were similar to curve of pure galena, and all of them exhibit an exothermic reaction. At the same adsorption time, adsorption curve peaks heightened and under-curve areas of galena bearing Ag, Bi and Cu impurities were higher and larger than those of pure galena curve, while these relationships for galena containing Mn, Zn and Sb impurities with pure galena were opposite.

Specific surface area, heat of adsorption and adsorption energy of xanthate on the impurity-doped galena are presented in Table 3. The crystalline properties of galena, such as granularity and hardness, could be affected when the impurity-bearing galena was synthesized through precipitation method. The specific surface area of galena containing various impurities was different when they were ground to be smaller than 45 μm. From Table 3, the specific surface area of Cu-containing galena showed the maximum value of 21.37 m^2/g, while the Zn-containing galena revealed the minimum value of 3.56 m^2/g. In addition, the heat of adsorption of perfect galena was −0.28 J/m^2, while the heats of adsorption of Ag- and Bi-containing galena were −0.82 and −0.61 J/m^2, respectively. This indicated that Ag and Bi could promote the adsorption of xanthate on the galena surface, while other kinds of impurities inhibited the adsorption process. For Cu-containing impurity galena, although the peak area was larger than that of pure galena, its specific surface area was also large. Therefore, the adsorption energy per unit area was smaller than that of pure galena.

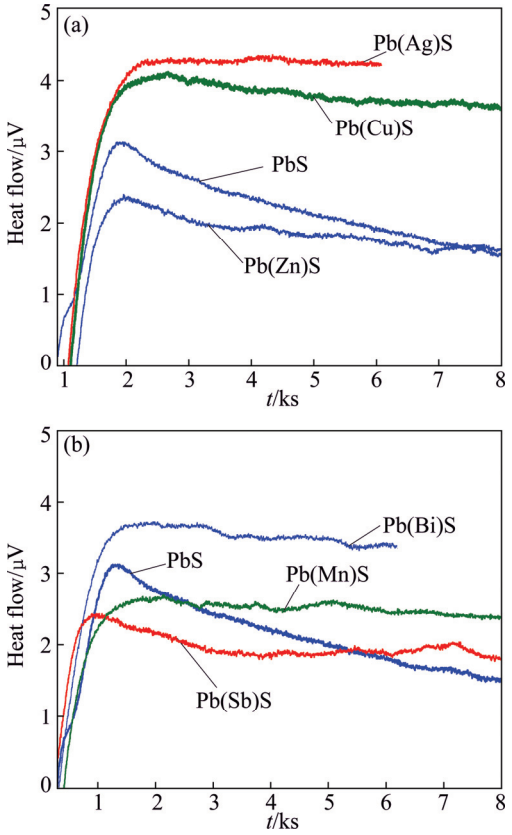

Fig. 8 Thermokinetic curves of BX adsorbed on surface of PbS containing Ag, Cu, Zn (a) and Bi, Mn, Sb (b) impurities

Table 3 Specific surface area, heat of adsorption and adsorption energy of xanthate on impurity-doped galena

Mineral	Specific surface area/(m^2·g^{-1})	Heat of adsorption, ΔH/(J·m^{-2})
PbS	9.35	−0.28
Pb(Ag)S	7.23	−0.82
Pb(Bi)S	5.24	−0.61
Pb(Cu)S	21.37	−0.18
Pb(Mn)S	5.81	−0.19
Pb(Sb)S	9.01	−0.17
Pb(Zn)S	3.56	−0.15

The directly proportional relationship between the absolute value of heat of adsorption and the flotation recovery of synthetic impurity-doped galena is shown in Fig. 9. For example, the heat of adsorption of the Ag-bearing galena was the largest, so its flotation recovery could achieve 100% using xanthate as collector, while the recovery of Zn-bearing galena was only 46%. The magnitude of the heat of adsorption could reflect the interaction strength of xanthate with impurity-doped galena surface. These observations provided information about the flotation behaviors of various kinds of impurity-bearing galena.

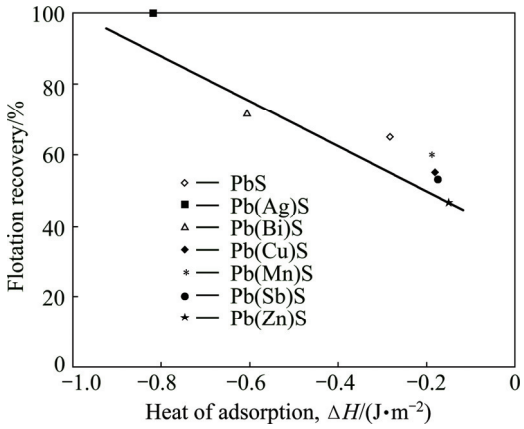

Fig. 9 Relationship between flotation recovery and heat of adsorption (ΔH) of synthetic impurity-doped galena

According to the basic thermodynamic formula, for an adsorption process, the Gibbs free energy can be defined as the following equation:

$$\Delta G=\Delta H-T\Delta S \tag{2}$$

where ΔH is the enthalpy, T is the temperature, and ΔS is the entropy (a measure of disorder). Because adsorption produces disorder in an orderly process, ΔS will be negative and consequently $-T\Delta S$, the second item in Eq. (2), will be positive. Therefore, ΔS will make a negative contribution to ΔG. The numerical value of Gibbs free energy depends mainly on the enthalpy ΔH, and the more negative value of ΔH results in the more negative value of ΔG, indicating easier occurrence of the adsorption reaction.

For impurity-doped galena surface, adsorption energy (ΔG) contains two parts, one is the adsorption energy of the impurity atom, the other is the adsorption energy of Pb atom. Therefore, the adsorption energy can be defined as Eq. (3):

$$\Delta G=\sum_{i=1}^{j}\Delta E_{\text{impurity}}+\sum_{i=j+1}^{n}\Delta E_{\text{Pb}} \tag{3}$$

where n is the number of adsorption sites, j is the number of impurity atoms of galena surface, $\Delta E_{\text{impurity}}$ is the adsorption energy of xanthate on the impurity atom, ΔE_{Pb} is the adsorption energy of xanthate on Pb atom, and ΔG is the total adsorption energy of xanthate. Therefore, the relationship between heat of adsorption and adsorption energy of the impurity atoms can be represented by Eq. (4):

$$\Delta H=\sum_{i=1}^{j}\Delta E_{\text{impurity}}+\sum_{i=j+1}^{n}\Delta E_{\text{Pb}}+T\Delta S \tag{4}$$

According to Eq. (4), the heat of adsorption of xanthate on the impurity-doped galena surface depends on the adsorption energy of impurities ($\Delta E_{\text{impurity}}$), the number of impurities on the galena surface (j) and the adsorption entropy change (ΔS). When similar quantities of impurities exist on the galena surface, the greater value of $\Delta E_{\text{impurity}}$ results in greater value of heat of adsorption. When the value of $\Delta E_{\text{impurity}}$ is constant, more impurity atoms lead to the greater value of the heat of adsorption, and greater value of ΔS produces the greater influence on the heat of adsorption.

The adsorption energies of the galena containing Cu, Bi and Zn were found well linearly related to the heat of adsorption (Eq. (5), R^2=0.9993). Compared Eq. (5) with Eq. (4), it was indicated that the number (j) of impurities on the galena surface and the entropy change (ΔS) were very similar to those of the galena samples containing Cu, Bi and Zn impurities. Thus, we conclude that the heat of adsorption of the xanthate adsorbed on the surface of these three kinds of impurities-bearing galena is mainly dependent on the interaction between the impurity atom and xanthate.

$$\Delta H=0.0032\ \Delta E_{\text{impurity}}+0.0737 \tag{5}$$

For the Ag-bearing galena, the adsorption energy of xanthate with Ag atom was −92.17 kJ/mol (see Table 2), which was not the most negative compared with those of the other impurity-bearing galena samples. However, the greatest heat of adsorption was −0.82 J/m^2 for the Pb(Ag)S (see Table 3). According to Eq. (4), this observation can be explained from the increase of the number of impurities (j) in $\sum_{i=1}^{j}\Delta E_{\text{impurity}}$. The DFT study suggested that Ag impurity atoms were energetically favored to exist on the outermost surface. By using X-ray photoelectron spectroscopy (XPS) technique, high Ag content on the surface layer of the Ag-bearing galena was observed.

For the Mn- and Sb-bearing galena, the adsorption energies of xanthate are about −199 kJ/mol (see Table 2), but the heats of adsorption were −0.19 and −0.17 J/m^2, respectively (see Table 3). According to Eq. (4), the quantities of Mn and Sb impurities were few on the galena surface and consequently weakened the thermal effect of the adsorption. In addition, the electron number of the 3d orbital is half full for the Mn atom, and it is also the same for the 5p orbital of Sb atoms. So, they exhibit a larger magnetic moment. This would enhance the oxidation of galena and weaken the adsorption of xanthate on the galena surface.

3.6 Effects of impurities on adsorption kinetics of xanthate on galena surface

Thermodynamics and kinetics are two factors that affect reaction rates. However, thermodynamics has no direct correlation with reaction rates, and the rate of an actual reaction mainly depends on the kinetics. The presence of impurities on the galena surface would

change the adsorption rate of the xanthate, hence the kinetic parameters of galena bearing different impurities were tested by means of the microcalorimetry technique.

The adsorption of xanthate on galena surface is approximated as irreversible chemical adsorption reaction, and Eq. (6) [31] can be used to calculate the rate coefficients and reaction order for the adsorption reaction:

$$\ln\left(\frac{1}{H_0}\frac{\mathrm{d}H_i}{\mathrm{d}t}\right)=\ln k+n\ln\left(1-\frac{H_i}{H_0}\right) \tag{6}$$

When the values of $\ln\left(\frac{1}{H_0}\frac{\mathrm{d}H_i}{\mathrm{d}t}\right)$ are plotted as a function of $\ln\left(1-\frac{H_i}{H_0}\right)$ values, the intercept and slope of the line present ln k and n, respectively. The adsorption rate coefficients (k) and adsorption orders (n) for xanthate adsorbed on different impurity-doped galena surfaces are listed in Table 4.

Table 4 Thermal kinetic parameters of xanthate adsorption on synthetic impurity-doped galena surface and flotation recovery

Mineral	Recovery/%	Thermal kinetic parameter	
		Rate coefficient, $k/10^{-3}\ \mathrm{s}^{-1}$	Reaction order, n
PbS	65.3	5.22	0.278
Pb(Ag)S	100	5.87	0.93
Pb(Bi)S	72.4	5.36	0.75
Pb(Cu)S	55.7	0.021	1.32
Pb(Mn)S	64.7	2.92	1.11
Pb(Sb)S	52.9	0.583	1.24
Pb(Zn)S	46.6	0.019	1.30

It can be seen from Table 4 that the reaction order (n) ranges from 0.2 to 1.3 for various impurity-bearing galena samples, hence, the adsorption of xanthate can be taken as the nearly first-order reaction. In other words, the adsorption of xanthate on the galena surface is proportional to the concentration. In addition, the reaction order of perfect galena is the smallest, indicating that impurities can increase the reaction order of xanthate adsorbed on the galena surface.

The adsorption rate coefficient (k) reflects the adsorption rate under the same temperature and adsorption reaction order. The k values of Ag-, Bi- and Mn-bearing galena are larger, resulting in greater flotation recovery. While k values of Cu-, Sb- and Zn-bearing galena are smaller, resulting in lower flotation recovery. It is found that the k and n values of Cu-bearing galena are very close to those of Zn-bearing galena, and their k values are even smaller than that of Sb-bearing galena; however, the flotation recovery of Cu-bearing galena is higher than those of Zn- and Sb-bearing galena. This abnormal phenomenon could be ascribed to the largest specific surface area of Cu-bearing galena (Table 3), which results in long time for xanthate to reach the adsorption equilibrium. In addition, the heat of adsorption of Cu-bearing galena is larger than that of Zn- and Sb-bearing galena, indicating that the interaction of xanthate with Cu-bearing galena is stronger than that of Zn- and Sb-bearing galena.

4 Conclusions

1) The XRD pattern illustrated that the lattice constant of synthetic PbS was very close to that of the natural galena and the values for both constants were very similar to the values reported in the literature. Moreover, the effects of Ag, Cu, Zn, Mn, Bi and Sb impurities on the lattice constant of galena were in agreement with the calculated values from DFT, confirming the reliability of crystal model and calculation parameters used in this study.

2) Specific surface area of synthetic galena was much larger than that of natural galena. Floatation experimental results showed that Ag and Bi impurities could significantly increase the galena recovery, while Zn, Sb, Mn and Cu impurities reduced the flotation recovery of galena. Zinc impurity could dramatically reduce the flotation recovery.

3) Microthermokinetic results showed that the relationship between adsorption microcalorimetry of xanthate and its flotation recovery was directly proportional to the impurity-doped galena surface. The heat of adsorption and reaction rate coefficients were larger when xanthate was adsorbed on the galena surface bearing Ag or Bi impurity; thus, their flotation recoveries were found to be greater. While for galena bearing Cu or Sb, the heat of adsorption and rate coefficients were smaller, resulting in lower flotation recoveries.

References

[1] HU Xi-geng. Non-ferrous metal sulfide ore dressing [M]. Beijing: Metallurgical Industry Press, 1987. (in Chinese)

[2] CHEN Jia-mo. Polymetallic sulphide flotation separation [M]. Guizhou: Guizhou Science and Technology Press, 2001. (in Chinese)

[3] AREHART G B, ELDRIDGE C S, CHRYSSOULIS S L, KESLER S E. Ion microprobe determination of sulfur isotope variations in iron sulfides from the Post/Betze sediment-hosted disseminated gold deposit [J]. Geochimica et Cosmochimica Acta, 1993, 57: 1505−1519.

[4] OUBERTH(U)R T, CABRI L J, WEISER T W, MCMAHON G, MULLER P. Pt, Pd and other trace elements in sulfides of the main sulfide zone, Great Dyke, Zimbabwe: A reconnaissance study [J]. Canadian Mineralogist, 1997, 35: 597−609.

[5] HUSTON D L, SIE S H, SUTER G F, COOKE D R, BOTH R A. Trace elements in sulfide minerals from Eastern Australian volcanic-hosted massive sulfide deposits: Part I. Proton microprobe analyses of pyrite, chalcopyrite, and sphalerite; Part II. Selenium

levels in pyrite: Comparison with $\delta^{34}S$ values and implications for the source of sulfur in volcanogenic hydrothermal systems [J]. Economic Geology, 1995, 90: 1167−1196.
[6] LI Yu-qiong, CHEN Jian-hua, CHEN Ye, GUO Jin. Density functional theory study of the influence of impurity on electronic properties and reactivity of pyrite [J]. Transactions of Nonferrous Metals Society of China, 2011, 21(8): 1887−1895.
[7] LI Yu-qiong, CHEN Jian-hua, GUO Jin. DFT study of influences of As, Co and Ni impurities on pyrite (100) surface oxidation by O_2 molecule [J]. Chemical Physics Letters, 2011, 511(4−6): 389−392.
[8] CHEN Ye, CHEN Jian-hua, GUO Jin. A DFT study on the effect of lattice impurities on the electronic structures and floatability of sphalerite [J]. Minerals Engineering, 2010, 23: 1120−1130.
[9] CHEN Ye, CHEN Jian-hua. The first-principle study of the effect of lattice impurity on adsorption of CN on sphalerite surface [J]. Minerals Engineering, 2010, 23: 676−684.
[10] CHEN Ye, CHEN Jian-hua, LAN Li-hong, YANG Mei-jin. The influence of the impurities on the flotation behaviors of synthetic ZnS [J]. Minerals Engineering, 2012, 27−28: 65−71.
[11] CHEN Jian-hua, WANG Lei, CHEN Ye, GUO Jin. A DFT study of the effect of natural impurities on the electronic structure of galena [J]. International Journal of Mineral Processing, 2011, 98: 132−136.
[12] LAAJALEHTO K, SUONINENA E, HEIMALAB S. Studies of the effect of antimony impurity on the flotation behaviour of galena [J]. International Journal of Mineral Processing, 1991, 33(1−4): 95−102.
[13] MELLGREN O. Heat of adsorption and surface reactions of potassium ethyl xanthate on galena [J]. Transactions Society of Mining Engineers, 1966, 235: 46−59.
[14] HAUNG H H, MILLER J D. Kinetics and thermochemistry of amyl xanthate adsorption by pyrite and marcasite [J]. International Journal of Mineral Processing, 1978, 5: 241−266.
[15] MAIER G S, QIU X, DOBIAS B. New collectors in the flotation of sulphide minerals: A study of the electrokinetic, calorimetric and flotation properties of sphalerite, galena and chalcocite [J]. Physicochemical and Engineering Aspects, 1997, 122: 207−225.
[16] Rock and Mineral Analysis Group. Petrographic and mineral analysis [M]. 3rd ed. Beijing: Geology Press, 1991. (in Chinese)
[17] SOLECKI J, KOMOSA A, SZCZYPA J. Copper ion activation of synthetic sphalerites with various iron contents [J]. International Journal of Mineral Processing, 1979, 6(3): 221−228.
[18] SZCZYPA J, SOLECKI J, KOMOSA A. Effect of surface oxidation and iron contents on xanthate ions adsorption of synthetic sphalerites [J]. International Journal of Mineral Processing, 1980, 7(2): 151−157.
[19] CHEN Jian-hua, KE Bao-lin, LAN Li-hong, LI Yu-qiong. Influence of Ag, Sb, Bi and Zn impurities on electrochemical and flotation behaviour of galena [J]. Minerals Engineering, 2015, 72: 10−16.
[20] CHEN Jian-hua, LAN Li-hong, CHEN Ye, GUO Jin. Computational simulation of adsorption and thermodynamic study of xanthate, dithiophosphate and dithiocarbamate on galena and pyrite surfaces [J]. Minerals Engineering, 2013, 46−47: 136−143.
[21] JI M, LIU M Y, GAO S L, SHI Q Z. A new microcalorimeter for measuring thermal effects [J]. Instrumentation Science and Technology, 2001, 29(1): 53−57.
[22] PAYNE M C, TETER M P, ALLAN D C, ARIAS T A, JOANNOPOULOS J D. Iterative minimization techniques for ab initio total energy calculation: Molecular dynamics and conjugate gradients [J]. Review of Modern Physics, 1992, 64: 1045−1097.
[23] PERDEW J P, WANG Y. Accurate and simple analytic representation of the electron–gas correlation energy [J]. Physical Review B, 1992, 45: 13244−13249.
[24] VANDERBILT D. Soft self-consistent pseudopotentials in a generalized eigenvalue formalism [J]. Physical Review B, 1990, 41: 7892−7895.
[25] MONKHORST H J, PACK J D. Special points for Brillouin-zone integrations [J]. Physical Review B, 1976, 13: 5188−5192.
[26] LI Yu-qiong, CHEN Jian-hua, LAN Li-hong, GUO Jin. The adsorption of O_2 on pyrite and galena surfaces [J]. The Chinese Journal of Nonferrous Metals, 2012, 22(4): 1184−1194. (in Chinese)
[27] LAN Li-hong, CHEN Jian-hua, LI Yu-qiong, CHEN Ye, GUO Jin. Effect of vacancy defects on oxygen molecule adsorption on galena surface (100) [J]. The Chinese Journal of Nonferrous Metals, 2012, 22(9): 2626−2635. (in Chinese)
[28] WASSERSTEIN B. Precision lattice measurements of galena [J]. American Mineralogist, 1951, 36: 102−115.
[29] WU Chui-zhi. Study on the flotation behavior and its mechanism of artificial magnetite and natural magnetite [D]. Nanning: Guangxi University, 2012. (in Chinese)
[30] FENG Qi-ming, CHEN Jian-hua. Electrochemistry of sulfide mineral flotation [M]. Changsha: Central South University Press, 2014:14−90. (in Chinese)
[31] GAO Sheng-li, CHEN San-ping, HU Rong-zu, LI Huan-yong, SHI Qi-zhen. Derivation and application of thermodynamic equations [J]. Chinese Journal of Inorganic Chemistry, 2002, 18: 362−366. (in Chinese)

含杂质方铅矿吸附黄药的微量热动力学研究

蓝丽红[1]，陈建华[2]，李玉琼[2]，蓝 平[1]，杨 卓[1]，艾光湧[1]

1. 广西民族大学 化学化工学院，广西高校化学与生物转化过程新技术重点实验室，南宁 530006；
2. 广西大学 资源与冶金学院，南宁 530004

摘 要：采用沉淀法合成 6 种不同掺杂方铅矿，并通过浮选实验考察杂质对方铅矿浮选性能的影响；采用微量热法测量含不同杂质原子的方铅矿表面吸附黄药的热力学和动力学参数；采用密度泛函理论对黄药分子在不同掺杂方铅矿表面的吸附构型和吸附能进行模拟计算。浮选实验结果表明：银、铋杂质能够显著提高方铅矿的回收率，而锌、锑、锰、铜杂质降低了方铅矿的浮选回收率。微量热动力学结果表明：含杂质方铅矿的吸附热与浮选回收率呈正比关系。黄药在含银和铋方铅矿表面的吸附热和反应速率常数均比纯方铅矿的大，对应的浮选回收率较高，而含铜和含锑方铅矿的吸附热和反应速率常数均比纯方铅矿的小，对应的浮选回收率较低。同时还分析了黄药在掺杂方铅矿表面的不饱和吸附热和黄药在杂质原子上的吸附能的关系。

关键词：方铅矿；杂质影响；浮选；黄药；吸附；微量热法；密度泛函理论

(Edited by Wei-ping CHEN)